

**PHOTOCATALYTIC DEGRADATION OF PHENOL AND
2,4-DICHLOROPHENOL USING RARE EARTH-DOPED ZnO
HIERARCHICAL MICRO/NANOSPHERES UNDER
FLUORESCENT LIGHT AND SUNLIGHT IRRADIATION**

by

SIN JIN CHUNG

**Thesis submitted in fulfillment of the requirements
for the degree of
Doctor of Philosophy**

AUGUST 2014

ACKNOWLEDGEMENTS

First and foremost, my deepest gratitude goes to my main supervisor, Prof. Dr. Abdul Rahman Mohamed for his valuable ideas, advices and guidance throughout my postgraduate studies. I would also grateful to my co-supervisor, Assoc. Prof. Dr. Lee Keat Teong for his support throughout the work.

Sincere thanks are also extended to management, most especially the Dean, Prof. Dr. Azlina Bt. Harun @ Kamaruddin, Deputy Dean, Assoc Prof. Dr. Ahmad Zuhairi Abdullah and all the staff members of School of Chemical Engineering, Universiti Sains Malaysia for their help and support. Besides that, I would also like to express my heartfelt thanks to Prof. Dr. Tadashi Itoh and Assoc. Prof. Dr. Ichikawa Satoshi for helping me operated high-resolution transmission electron microscopy analyses at Institute for NanoScience Design, Osaka University. My appreciation also goes to the staffs at School of Material and Mineral Resources Engineering, School of Biology and School of Chemical Science, Universiti Sains Malaysia for the help with sample analyses.

Special appreciation also goes to Malaysia government for providing me the MyPhD scholarship throughout my postgraduate studies. At the same time, I also appreciated the Universiti Sains Malaysia for funding my project via a Research Universiti grant (no. 814176) and a Postgraduate Research Scheme (no. 8045032).

Finally, I would like to express my sincere gratitude to my parent Sin Boon Hwa and Ang Cheong Sim, brother Sin Jin Ming and sisters Sin Min Chyi and Sin Yuh Miin and my beloved friends especially Lam Sze Mun, Yeoh Wei Ming, Seah Choon Ming, Lee Kim Yang and Rohaiya for their continuous supports and encouragement to complete this work.

TABLE OF CONTENTS

	Page
ACKNOWLEDGEMENTS	ii
TABLE OF CONTENTS	iii
LIST OF TABLES	ix
LIST OF FIGURES	x
LIST OF PLATES	xvii
LIST OF SYMBOLS	xviii
LIST OF ABBREVIATIONS	xx
ABSTRAK	xxii
ABSTRACT	xxiv
CHAPTER ONE : INTRODUCTION	
1.1 Wastewater treatment	1
1.2 Photocatalysis in wastewater treatment	4
1.3 Problem statement	6
1.4 Research objectives	8
1.5 Scope of study	9
1.6 Organization of the thesis	10
CHAPTER TWO : LITERATURE REVIEW	
2.1 Endocrine disrupting chemicals	12
2.1.1 Phenol	14
2.1.2 2,4-dichlorophenol (2,4-DCP)	17

2.2	Heterogeneous photocatalysis	19
2.3	ZnO as a photocatalyst	21
2.3.1	Basic knowledge of ZnO	22
2.3.2	Mechanism of ZnO-assisted photocatalysis	25
2.4	Modification of ZnO	29
2.4.1	ZnO at nanoscale and complex hierarchical micro/nanostructure	30
2.4.2	Modification with rare earth doping	39
2.5	Synthesis of ZnO hierarchical architectures	45
2.6	Effects of operating parameters	49
2.6.1	Effect of initial pollutant concentration	50
2.6.2	Effect of solution pH	52
2.6.3	Effect of light intensity and wavelength	58
2.7	Analysis and identification of intermediates	60
2.7.1	Phenol and its degradation intermediates	61
2.7.2	2,4-DCP and its degradation intermediates	62
2.8	Summary of literature review	64

CHAPTER THREE : MATERIALS AND METHODS

3.1	Materials and chemicals	67
3.2	Equipments	68
3.2.1	Stainless steel Teflon-lined autoclave	68
3.2.2	Photocatalytic experiment setup	69
3.3	Photocatalyst preparation	72

3.3.1	Preparation of ZnO hierarchical micro/nanospheres based photocatalysts	72
3.3.2.	Preparation of one-dimensional ZnO nanorods (ZNRs)	73
3.4	Characterization studies	75
3.4.1	X-ray diffraction (XRD)	75
3.4.2	Scanning electron microscopy (SEM) and energy dispersive X-ray (EDX) spectroscopy	75
3.4.3	Transmission electron microscopy (TEM) and high-resolution transmission electron microscopy (HRTEM)	75
3.4.4	UV-visible diffuse reflectance (UV-vis DRS) spectroscopy	76
3.4.5	Nitrogen adsorption-desorption analysis	76
3.4.6	Photoluminescence (PL) emission spectra	77
3.5	Photocatalytic performance evaluation	77
3.5.1	Effect of rare earth (RE) doping	78
3.5.2	Detection of active species	79
3.5.3	Effect of calcination temperature	79
3.5.4	Reusability of the photocatalysts	80
3.5.5	Intermediates detection studies	80
3.6	Effects of operating parameters	80
3.6.1	Effect of initial substrate concentration	80
3.6.2	Effect of solution pH	81
3.7	Kinetic study	81
3.8	Sample analyses	82
3.8.1	High performance liquid chromatograph (HPLC)	82

3.8.2	Zeta potential	82
3.8.3	Metal leaching analysis	83
3.8.4	Total organic carbon (TOC)	83
3.8.5	Ion chromatography (IC)	84

CHAPTER FOUR : RESULTS AND DISCUSSION

4.1	Characterization of the as-synthesized photocatalysts	86
4.1.1	X- ray diffraction (XRD)	86
4.1.2	Scanning electron microscopy (SEM)	90
4.1.3	Energy dispersive X-ray (EDX)	94
4.1.4	Transmission electron microscopy (TEM) and high- resolution transmission electron microscopy (HRTEM)	95
4.1.5	UV-visible diffuse reflectance spectroscopy (UV-vis DRS)	98
4.1.6	Nitrogen adsorption-desorption	101
4.2	Formation of the hierarchical micro/nanospheres	108
4.3	Photocatalytic degradation of phenol using different photocatalysts	111
4.4	Effect of rare earth doping on the photocatalytic performance	115
4.5	Effect of rare earth doping content on the photocatalytic performance	118
4.6	Proposed photocatalytic mechanism	121
4.6.1	Photoluminescence (PL) emission analysis	121
4.6.2	Active species responsible for photocatalytic degradation	123

4.6.3	Proposed degradation mechanism and the role of RE dopant	129
4.7	Effect of calcination temperature on the photocatalytic activity of Nd/ZnO	131
4.8	Effects of operating parameters	134
4.8.1	Effect of initial phenol concentration	134
4.8.2	Effect of solution pH	135
4.9	Reusability of the photocatalyst	139
4.10	Photocatalytic degradation of 2,4-dichlorophenol	142
4.10.1	Comparison of different photocatalysts	142
4.10.2	Effect of initial 2,4-DCP concentration	144
4.10.3	Effect of solution pH	145
4.11	Intermediate products and mineralization evaluation upon phenol and 2,4-DCP degradation	147
4.11.1	HPLC analysis for phenol degradation	147
4.11.2	The variation of TOC in phenol degradation	150
4.11.3	HPLC analysis for 2,4-DCP degradation	151
4.11.4	The variation of TOC and IC in 2,4-DCP degradation	154
4.12	Kinetics study	156
4.12.1	Determining the kinetic order	156
4.12.2	Langmuir-Hinshelwood model	160
4.12.3	Initial reaction rate	162
4.13	Electrical energy efficiency	164
4.14	Sunlight degradation of phenol and 2,4-DCP	166

CHAPTER FIVE: CONCLUSIONS AND RECOMMENDATIONS	
5.1 Conclusions	169
5.2 Recommendations	173
REFERENCES	174
APPENDIX	208
LIST OF PUBLICATIONS	221

LIST OF TABLES

		Page
Table 2.1	Chemical and physical properties of phenol (Busca <i>et al.</i> , 2008)	15
Table 2.2	Chemical and physical properties of 2,4-DCP (Pohanish, 2012)	18
Table 2.3	List of organic pollutants degraded by ZnO photocatalysis	28
Table 2.4	ZnO at nanoscale and complex hierarchical micro/nanostructures on the photocatalytic degradation of various organic pollutants	32
Table 2.5	Effect of RE doping on the ZnO photocatalytic activity	44
Table 2.6	Methods to prepare the ZnO hierarchical architectures	45
Table 2.7	Effect of solution pH on the photocatalytic degradation of various organic pollutants	54
Table 3.1	List of chemical and materials	67
Table 4.1	Crystal analysis of different photocatalysts	89
Table 4.2	Band gap energies of different photocatalysts	101
Table 4.3	BET surface area and porosity parameters of different photocatalysts	106
Table 4.4	Comparison of the results obtained in this study with previous results from degradation of phenol	114
Table 4.5	Reaction order and rate law for a reaction involving a single reactant (Fogler, 1999)	156
Table 4.6	Values of k and R^2 under different initial substrate concentrations	160
Table 4.7	Electrical energy efficiency during photocatalytic degradation of phenol and 2,4-DCP over different photocatalysts under fluorescent light irradiation. Conditions: catalyst loading = 1.0 g/L, [phenol/2,4-DCP] = 20 mg/L, $\text{pH}_{\text{phenol}} = 5.6$ and $\text{pH}_{2,4\text{-DCP}} = 5.9$	166

LIST OF FIGURES

		Page
Figure 1.1	Different wastewater treatment technologies currently in use in environmental remediation (Visvanathan <i>et al.</i> , 2005; Mohan and Pittman, 2006; An <i>et al.</i> , 2010)	3
Figure 2.1	Endocrine disruption processes: (a) Natural response, (b) agonistic effect and (c) antagonistic effect (Birkett and Lester, 2003)	13
Figure 2.2	Photoactivation of the electron within the bandgap (Gaya and Abdullah, 2008)	19
Figure 2.3	Schematic photoexcitation of the semiconductor photocatalyst and the following redox reactions (Koči <i>et al.</i> , 2008)	21
Figure 2.4	The CB and VB positions of some common semiconductor photocatalysts and their band gap energy (Liu <i>et al.</i> , 2014)	22
Figure 2.5	Ball and stick representation of ZnO crystal structures: (a) cubic rocksalt; (b) cubic zinc blende; (c) hexagonal wurtzite. The shaded white and black spheres denote Zn and O atoms, respectively (Özgür <i>et al.</i> , 2005)	24
Figure 2.6	ZnO structured morphologies: (a) pencil-like ZnO microrods (Liu <i>et al.</i> , 2012a), (b) ZnO nanowires (Pyne <i>et al.</i> , 2012), (c) ZnO nanopellets (Chiu <i>et al.</i> , 2010), (d) ZnO micro-flowers (Wahab <i>et al.</i> , 2011), (e) hollow double-caged peanut-like ZnO hierarchical superstructures (Wang <i>et al.</i> , 2012a), (f) cuboid-shaped ZnO hierarchical structures (Wang <i>et al.</i> , 2010a), (g) ZnO tetrapods (Warule <i>et al.</i> , 2009), (h) lotus-like ZnO hierarchical structure (Yu <i>et al.</i> , 2011a) and (i) corn-like ZnO (Liu <i>et al.</i> , 2011b)	31
Figure 2.7	Photocatalytic activity of RE ion modified ZnO (Weber <i>et al.</i> , 2012)	40
Figure 2.8	A possible degradation mechanism of phenol (Thennarasu and Sivasamy, 2013)	61
Figure 2.9	A possible degradation mechanism of 2,4-DCP (Gaya <i>et al.</i> , 2010)	64
Figure 3.1	Flow chart of experimental work involved in this study	66

Figure 3.2	Schematic diagram of stainless steel Teflon-lined autoclave. (1) Magnetic stirrer, (2) Teflon, (3) ZnO colloidal solution, (4) Stainless steel plate, (5) Magnetic bar, (6) Heater, (7) Insulator, (8) Stainless steel cap, (9) Nut, (10) Pressure gauge, (11) Thermocouple, (12) Pressure release valve and (13) Nut	69
Figure 3.3	Schematic diagram of photocatalytic system under fluorescent light irradiation. (1) Air pump, (2) Flow meter, (3) Air supply, (4) Compact fluorescent lamp, (5) Suspension, (6) Magnetic bar, (7) Hot plate stirrer, (8) Acrylic black box and (9) Cooling fans	70
Figure 3.4	Schematic diagram of photocatalytic system under sunlight irradiation. (1) Air pump, (2) Retort stand, (3) Flow meter, (4) Air supply, (5) Suspension, (6) Magnetic bar and (7) Hot plate stirrer	72
Figure 3.5	Flow chart of the preparation of RE/ZnO photocatalysts	73
Figure 3.6	Flow chart of the preparation of ZNRs photocatalysts	74
Figure 4.1	XRD patterns for (a) Ce/ZnO, (b) Eu/ZnO and (c) Nd/ZnO with different doping contents	87
Figure 4.2	XRD patterns of Nd(2.0%)/ZnO treated at different calcination temperatures	90
Figure 4.3	SEM images of pure ZnO hierarchical micro/nanospheres calcined at 450°C. Magnification of (a) 1500 X, (b) 10000 X, (c) 40000 X and (d) 80000 X	91
Figure 4.4	SEM images of (a) Ce(2.0%)/ZnO, (b) Eu(2.0%)/ZnO, (c) Nd(2.0%)/ZnO and (d) Nd(3.0%)/ZnO calcined at 450°C with magnification of 40000 X	92
Figure 4.5	SEM images of Nd(2.0%)/ZnO calcined at (a) 550°C and (b) 650°C with magnification of 40000 X	93
Figure 4.6	EDX spectra of (a) Ce(2.0%)/ZnO, (b) Eu(2.0%)/ZnO, (c) Nd(2.0%)/ZnO and (d) Nd(3.0%)/ZnO photocatalysts	94
Figure 4.7	The elemental mapping images of (a) Ce(2.0%)/ZnO, (b) Eu(2.0%)/ZnO and (c) Nd(2.0%)/ZnO photocatalysts	95
Figure 4.8	TEM images of (a) pure ZnO, (b) Ce(2.0%)/ZnO, (c) Eu(2.0%)/ZnO and (d) Nd(2.0%)/ZnO photocatalysts	96

Figure 4.9	HRTEM images of (a) pure ZnO, (b) Ce(2.0%)/ZnO, (c) Eu(2.0%)/ZnO and (d) Nd(2.0%)/ZnO photocatalysts	97
Figure 4.10	UV-vis DRS spectra of (a) pure ZnO, ZNRs and RE(2.0%)/ZnO; (b) Nd/ZnO with different Nd doping contents	99
Figure 4.11	Plot of % reflectance versus photon energy. (a) pure ZnO, ZNRs and RE(2.0%)/ZnO; (b) Nd/ZnO with different Nd doping contents	101
Figure 4.12	N ₂ adsorption-desorption isotherms and the corresponding pore size distribution curve (inset) of as-synthesized (a) pure ZnO and (b) ZNRs	103
Figure 4.13	N ₂ adsorption-desorption isotherms and the corresponding pore size distribution curve (inset) of as-synthesized (a) Ce(2.0%)/ZnO, (b) Eu(2.0%)/ZnO, (c) Nd(2.0%)/ZnO and (d) Nd(3.0%)/ZnO photocatalysts	105
Figure 4.14	N ₂ adsorption-desorption isotherms and the corresponding pore size distribution curve (inset) of as-synthesized Nd(2.0%)/ZnO calcined at (a) 550°C and (b) 650°C	107
Figure 4.15	SEM images of the samples collected at different growth stages: (a) 5 min; (b) 30 min; (c) 90 min and (d) 180 min	109
Figure 4.16	Schematic illustration of the formation process of ZnO hierarchical micro/nanospheres	111
Figure 4.17	Removal of phenol under different conditions. Conditions: catalyst loading = 1.0 g/L, [phenol] = 20 mg/L and solution pH = 5.6	112
Figure 4.18	Photocatalytic degradation of phenol using pure ZnO and different RE(2.0%)/ZnO photocatalysts. Conditions: catalyst loading = 1.0 g/L, [phenol] = 20 mg/L and solution pH = 5.6	116
Figure 4.19	Photocatalytic degradation of phenol over RE/ZnO with different RE doping contents: (a) Ce/ZnO, (b) Eu/ZnO and (c) Nd/ZnO. Conditions: catalyst loading = 1.0 g/L, [phenol] = 20 mg/L and solution pH = 5.6	119
Figure 4.20	PL spectra of pure ZnO and RE(2.0%)/ZnO photocatalysts	122

Figure 4.21	PL spectra of RE/ZnO with different doping contents: (a) Ce/ZnO, (b) Eu/ZnO and (c) Nd/ZnO	123
Figure 4.22	Effects of different 0.2mM scavengers on the degradation of phenol in the presence of RE(2.0%)/ZnO. Conditions: catalyst loading = 1.0 g/L, [phenol] = 20 mg/L and solution pH = 5.6	125
Figure 4.23	TA-PL spectra with an excitation of 315 nm under different photocatalysts for 180 min	127
Figure 4.24	TA-PL spectra changing with irradiation time for the case of the Nd(2.0%)/ZnO photocatalysts	128
Figure 4.25	Proposed photocatalytic mechanism of RE/ZnO photocatalysts	130
Figure 4.26	Photocatalytic activity of Nd(2.0%)/ZnO treated at different calcination temperatures. Conditions: catalyst loading = 1.0 g/L, [phenol] = 20 mg/L and solution pH = 5.6	132
Figure 4.27	Effect of initial phenol concentration on the photocatalytic degradation of phenol over Nd(2.0%)/ZnO. Conditions: catalyst loading = 1.0 g/L and solution pH = 5.6	134
Figure 4.28	Effect of solution pH on photocatalytic degradation of phenol over Nd(2.0%)/ZnO. Conditions: catalyst loading = 1.0 g/L and [phenol] = 20 mg/L	136
Figure 4.29	Zeta potential analysis of Nd(2.0%)/ZnO as a function of pH	138
Figure 4.30	Photocatalytic activity of the Nd(2.0%)/ZnO for phenol degradation with three times of cycling uses. Conditions: [phenol] = 20 mg/L and solution pH = 5.6	140
Figure 4.31	Photographs of sedimentation for 2 h in aqueous suspensions of (a) Nd(2.0%)/ZnO and (b) commercial TiO ₂	142
Figure 4.32	2,4-DCP concentration dependence on irradiation time using various photocatalysts. Conditions: catalyst loading = 1.0 g/L, [2,4-DCP] = 20 mg/L and solution pH = 5.9	143

Figure 4.33	Effect of initial 2,4-DCP concentration on the photocatalytic degradation of 2,4-DCP over Nd(2.0%)/ZnO. Conditions: catalyst loading = 1.0 g/L and solution pH = 5.9	145
Figure 4.34	Effect of solution pH on the photocatalytic degradation of 2,4-DCP over Nd(2.0%)/ZnO. Conditions: catalyst loading = 1.0 g/L and [2,4-DCP] = 20 mg/L	146
Figure 4.35	Time-dependent HPLC chromatogram of phenol over Nd(2.0%)/ZnO. (a) before irradiation, (b) 60 min, (c) 180 min and (d) 300 min. Conditions: catalyst loading = 1.0 g/L, [phenol] = 20 mg/L and solution pH = 5.6	148
Figure 4.36	Proposed reaction pathway for photodegradation of aqueous phenol by the Nd(2.0%)/ZnO	150
Figure 4.37	Photocatalytic degradation and TOC removal of phenol over the Nd(2.0%)/ZnO. Conditions: catalyst loading = 1.0 g/L, [phenol] = 20 mg/L and solution pH = 5.6	151
Figure 4.38	Time-dependent HPLC chromatogram of 2,4-DCP over Nd(2.0%)/ZnO. (a) before irradiation, (b) 60 min, (c) 120 min and (d) 180 min. Conditions: catalyst loading = 1.0 g/L, [2,4-DCP] = 20 mg/L and solution pH = 5.9	152
Figure 4.39	Proposed reaction pathway for photodegradation of aqueous 2,4-DCP by the Nd(2.0%)/ZnO	154
Figure 4.40	Variation of degradation efficiency, TOC removal and Cl ⁻ ion concentration during the 2,4-DCP degradation. Conditions: catalyst loading = 1.0 g/L, [2,4-DCP] = 20 mg/L and solution pH = 5.9	155
Figure 4.41	Fitting for zero-order reaction. Conditions: catalyst loading = 1.0 g/L, [phenol or 2,4-DCP] = 20 mg/L, pH _{phenol} = 5.6 and pH _{2,4-DCP} = 5.9	157
Figure 4.42	Fitting for first-order reaction. Conditions: catalyst loading = 1.0 g/L, [phenol or 2,4-DCP] = 20 mg/L, pH _{phenol} = 5.6 and pH _{2,4-DCP} = 5.9	157
Figure 4.43	Fitting for second-order reaction. Conditions: catalyst loading = 1.0 g/L, [phenol or 2,4-DCP] = 20 mg/L, pH _{phenol} = 5.6 and pH _{2,4-DCP} = 5.9.	158

Figure 4.44	Fitting for third-order reaction. Conditions: catalyst loading = 1.0 g/L, [phenol or 2,4-DCP] = 20 mg/L, $\text{pH}_{\text{phenol}} = 5.6$ and $\text{pH}_{2,4\text{-DCP}} = 5.9$	158
Figure 4.45	Plot of $\ln C_0/C$ versus time for phenol degradation under different initial phenol concentrations. Conditions: catalyst loading = 1.0 g/L and solution pH = 5.6	159
Figure 4.46	Plot of $\ln C_0/C$ versus time for 2,4-DCP degradation under different initial 2,4-DCP concentrations. Conditions: catalyst loading = 1.0 g/L and solution pH = 5.9	160
Figure 4.47	Initial rate plot ($1/r_0$ against $1/C_0$) for photocatalytic degradation of phenol via Nd(2.0%)/ZnO	163
Figure 4.48	Initial rate plot ($1/r_0$ against $1/C_0$) for photocatalytic degradation of 2,4-DCP via Nd(2.0%)/ZnO	163
Figure 4.49	Photocatalytic degradation of phenol and 2,4-DCP under fluorescent light (irradiation time = 30 min) and sunlight (irradiation time = 15 min) over different photocatalysts. Conditions: catalyst loading = 1.0 g/L, [phenol/2,4-DCP] = 20 mg/L, $\text{pH}_{\text{phenol}} = 5.6$ and $\text{pH}_{2,4\text{-DCP}} = 5.9$	167
Figure A-1	Calibration curve for phenol of HPLC analysis. HPLC conditions: wavelength = 254 nm; mobile phase = mixture of water and acetonitrile in the ratio of 70:30; flow rate = 1 mL/min	208
Figure A-2	Calibration curve for 2,4-DCP of HPLC analysis. HPLC conditions: wavelength = 280 nm; mobile phase = mixture of acetonitrile, acetic acid and water in the ratio of 69:1:30; flow rate = 1 mL/min	209
Figure A-3	Calibration curve for Zn^{2+} solution of AAS analysis. AAS condition: wavelength = 213.5 nm.	210
Figure A-4	Calibration curve for chloride ion of IC analysis. IC conditions: mobile phase = 1.7 mM HNO_3 with 0.7 mM dipicolinic acid; flow rate = 0.7 mL/min	211
Figure A-5	XRD pattern of solvothermally synthesized pure ZNRs	212
Figure A-6	SEM images of solvothermally synthesized pure ZNRs. Magnification of (a) 10000 X and (b) 60000 X	213

Figure A-7	SEM image of Nd(2.0%)/ZnO treated at 450°C after reused for three cycles	214
Figure A-8	HPLC chromatogram of muconic acid standard chemical for phenol degradation.	215
Figure A-9	HPLC chromatogram of resorcinol standard chemical for phenol degradation.	216
Figure A-10	HPLC chromatogram of benzoquinone standard chemical for phenol degradation.	217
Figure A-11	HPLC chromatogram of phenol standard chemical for 2,4-DCP degradation.	218
Figure A-12	HPLC chromatogram of 2-chlorophenol standard chemical for 2,4-DCP degradation.	219
Figure A-13	EDX spectrum of Nd(2.0%)/ZnO after the photocatalytic degradation of 2,4-DCP.	220

LIST OF PLATES

		Page
Plate 3.1	Stainless steel Teflon-lined autoclave	68
Plate 3.2	Picture of a laboratory scale batch photocatalytic system	71

LIST OF SYMBOLS

Symbol	Description	Unit
C	Pollutant concentration	mg/L
C_o	Initial pollutant concentration	mg/L
c	Velocity of light	m/s
D	Crystallite size	nm
e_{cb}^-	Conduction band electron	-
E	Band gap energy	eV
h	Planck's constant	eVs
H	Hysteresis type	-
h_{vb}^+	Valence band hole	-
$h\nu$	Photon energy	-
k	Observed rate constant	min ⁻¹
k_r	Reaction rate constant	mg/L•min
K_a	Adsorption constant	L/mg
$O_2\cdot^-$	Superoxide anion radical	-
OH^-	Hydroxyl ion	-
$\cdot OH$	Hydroxyl radical	-
P	Pressure	Pa
P_o	Initial pressure	Pa
pzc	Point of zero charge	-
R^2	Correlation coefficient	-
r	Reaction rate	mg/L•min
r_o	Initial reaction rate	mg/L•min

t	Time	min
β	Full width at half maximum	-
θ	Bragg angle	-
λ	Wavelength	nm

LIST OF ABBREVIATIONS

AAS	Atomic absorption spectrophotometer
AOPs	Advanced oxidation processes
BET	Brunauer-Emmett-Teller
CB	Conduction band
Ce	Cerium
CO ₂	Carbon dioxide
DI	Deionized water
EDCs	Endocrine disrupting chemicals
EDX	Energy dispersive X-ray spectroscopy
E_{EO}	Electrical energy per order
Eu	Europium
H ₂ SO ₄	Sulphuric acid
H ₂ O	Water
HNO ₃	Nitric acid
HPLC	High pressure liquid chromatograph
HRTEM	High-resolution transmission electron microscopy
IC	Ion chromatography
NaI	Sodium iodide
NaOH	Sodium hydroxide
Nd	Neodymium
NHE	Normal hydrogen electrode
N ₂	Nitrogen
O ₂	Oxygen
PL	Photoluminescence

BQ	<i>p</i> -benzoquinone
RE	Rare earth
RE/ZnO	Rare earth ion-doped zinc oxide
SEM	Scanning electron microscopy
TA	Terephthalic acid
TEM	Transmission electron microscopy
TiO ₂	Titanium dioxide
TOC	Total organic carbon
USEPA	United states environmental protection agency
UV	Ultraviolet
UV-vis DRS	Ultraviolet-visible diffuse reflectance spectroscopy
VB	Valence band
XRD	X-ray diffraction
ZnO	Zinc oxide
ZNRs	Zinc oxide nanorods
2,4-DCP	2,4-dichlorophenol
1D	One-dimensional
2D	Two-dimensional
3D	Three-dimensional

DEGRADASI PEMFOTOMANGKINAN FENOL DAN 2,4-DIKLOROFENOL MENGGUNAKAN HIERARKI ZnO BERBENTUK SFERA MIKRO/NANO TERDOP DENGAN NADIR BUMI DI BAWAH PENYINARAN CAHAYA PNDARFLUOR DAN CAHAYA MATAHARI

ABSTRAK

Kebimbangan berterusan ditambahkan terhadap kesan pendedahan kepada bahan kimia dengan aktiviti pengganggu endokrin. Setakat ini, pengasingan effluen bahan kimia pengganggu endokrin ke dalam sistem akuatik masih adalah satu cabaran yang rumit bagi banyak negara. Fotopemangkinan menggunakan hierarki ZnO baru-baru in ditampilkan sebagai teknologi yang cekap dan boleh dipraktikkan untuk rawatan air tercemar. Dalam kajian ini, hierarki ZnO berbentuk sfera mikro/nano terdop dengan ion nadir bumi (RE/ZnO, ion RE = Ce, Eu and Nd) telah disintesis dengan kaedah pemendakan kimia untuk fotodegradasi dua jenis bahan kimia pengganggu endokrin iaitu fenol dan 2,4-diklorofenol (2,4-DCP) di bawah penyinaran lampu pendarfluor dan cahaya matahari. Produk ZnO yang disintesis adalah berkristal dan terkumpul dengan banyak helai nano yang menyilang antara satu sama lain. Dopan nadir bumi mengalihkan penyerapan cahaya bagi ZnO ke kawasan gelombang yang lebih tinggi dan menurunkan jurang jalur. Kecekapan fotodegradasi fenol bagi hierarki ZnO berbentuk sfera mikro/nano didapati memberi keputusan yang lebih baik berbanding dengan ZnO berbentuk rod nano yang disintesis dengan kaedah solvoterma dan TiO₂ komersial di bawah penyinaran lampu pendarfluor. Fotoaktiviti ZnO juga dapat dipercepatkan oleh dopan nadir bumi. Nd/ZnO menunjukkan prestasi yang terbaik di antara RE/ZnO yang dikaji dalam

degradasi fenol di bawah penyinaran cahaya pendarfluor. Kepekatan dopan Ce, Eu dan Nd yang optimum untuk degradasi fenol adalah 1.5%, 2.0% dan 2.0% masing-masing. Selain itu, suhu pengkalsinan yang sesuai untuk Nd(2.0%)/ZnO adalah 450°C. Nd(2.0%)/ZnO yang dihasilkan juga menunjukkan potensi untuk kitar semula kerana ia boleh memendap di dalam larutan dalam masa dua jam selepas penyinaran dan fotoaktiviti mereka masih lebih daripada 77% selepas degradasi fenol selama tiga kali. 2,4-DCP juga berjaya didegradasi di bawah keadaan yang sama dengan menggunakan Nd(2.0%)/ZnO. Parameter operasi seperti kepekatan awal substrat dan pH larutan juga dikaji. Beberapa produk degradasi telah dikesan menggunakan kromatografi cecair prestasi tinggi (HPLC) bagi degradasi pemfotomangkinan fenol dan 2,4-DCP. Kinetik degradasi fenol dan 2,4-DCP mematuhi kinetik tertib-pertama diwakili oleh model Langmuir-Hinshelwood. Keputusan penggunaan tenaga elektrik untuk degradasi fenol dan 2,4-DCP menunjukkan bahawa Nd(2.0%)/ZnO adalah lebih cekap daripada ZnO tulen dan TiO₂ komersial dalam pengurangan kos tenaga untuk rawatan air sisa. Aktiviti pemfotomangkinan di bawah penyinaran cahaya matahari yang lebih baik juga ditunjukkan oleh Nd(2.0%)/ZnO berbanding dengan ZnO tulen dan TiO₂ komersial. Akhirnya, kecekapan degradasi 2,4-DCP didapati lebih tinggi daripada fenol di bawah penyinaran lampu pendarfluor dan cahaya matahari.

PHOTOCATALYTIC DEGRADATION OF PHENOL AND 2,4-DICHLOROPHENOL USING RARE EARTH-DOPED ZnO HIERARCHICAL MICRO/NANOSPHERES UNDER FLUORESCENT LIGHT AND SUNLIGHT IRRADIATION

ABSTRACT

Widespread concerns continue to be raised about the impacts of exposure to chemical compounds with endocrine disrupting activities. To date, the percolation of endocrine disrupting chemical (EDC) effluent into the aquatic system remains an intricate challenge abroad the nations. Heterogeneous photocatalysis using ZnO hierarchical architectures has recently been emerged as an efficient and feasible technology for the purification of polluted water. In this study, ZnO hierarchical micro/nanospheres doped with rare earth ion (RE/ZnO, RE ion = Ce, Eu and Nd) were synthesized using a chemical precipitation method for the photocatalytic degradation of two EDCs, namely phenol and 2,4-dichlorophenol (2,4-DCP) under fluorescent light and sunlight irradiation. The as-synthesized ZnO photocatalysts were well crystalline and accumulated by large amount of interleaving nanosheets. The RE doping shifted the light absorption of ZnO to longer wavelengths and narrowed the band gap. Under fluorescent light irradiation, the ZnO hierarchical micro/nanospheres exhibited excellent phenol degradation compared to the solvothermally synthesized ZnO nanorods and commercial TiO₂. The photocatalytic activity of the synthesized ZnO was further improved by doping with the studied RE ion. The Nd/ZnO exhibited the best performance in the fluorescent light degradation of phenol among the RE/ZnO samples. The optimum doping content of the Ce, Eu and Nd ions was found to be 1.5%, 2.0% and 2.0%, respectively. Moreover, the

adequate calcination temperature for Nd(2.0%)/ZnO was 450°C. The Nd(2.0%)/ZnO also showed favourable recycle use potential because they could settle out of solution within 2 h after irradiation and their photocatalytic activities were still more than 77% after three cycles of reaction. The 2,4-DCP were also successfully photodegraded under identical conditions over the Nd(2.0%)/ZnO. Operating parameters such as initial substrate concentration and solution pH were also investigated. Several degradation intermediates were also detected using high performance liquid chromatography (HPLC) on the photocatalytic degradation of phenol and 2,4-DCP. The kinetic analysis of the EDCs degradation over Nd(2.0%)/ZnO fitted well by first-order kinetics represented by the Langmuir-Hinshelwood model. The electrical energy per order results for EDCs degradation showed that the Nd(2.0%)/ZnO was useful than the pure ZnO and commercial TiO₂ in decreasing energetic cost of wastewater treatment. Under sunlight irradiation, considerable photocatalytic activities were also observed on the Nd(2.0%)/ZnO in comparison to pure ZnO and commercial TiO₂. Finally, the degradation efficiencies of 2,4-DCP were found to be higher than phenol under fluorescent light and sunlight irradiation.

CHAPTER ONE

INTRODUCTION

1.1 WASTEWATER TREATMENT

Water is one of the most important natural resources to every living thing in the world. With the rapid development of science and technology, many industries such as petrochemical, pharmaceutical, textile, mining and electronics are set up worldwide. Each of these industries required large quantity of water for daily activities and water released from these industries is contaminated with pollutants such as dyes, pharmaceuticals, surfactants and endocrine disrupting chemicals (EDCs) which have contributed to the contamination of fresh water in the ecosystem. Moreover, the increasing population of the world is escalating the requirements of clean water for drinking and household purposes. The high population density has also triggered large number of contaminants entering the water supply and contributed to exacerbate this problem. Furthermore, to fulfill the growing demand of food supply due to the high population growth, a lot of pesticides have been used in agricultural activities, which also violated the water supply and increased the water contamination (Robertson *et al.*, 2005).

The discovery of EDCs in the wastewater lately is being concerned. EDCs sources are mainly from the anthropogenic chemicals which have the ability to disrupt the healthy endocrine systems (Gültekin and Ince, 2007). Phenols such as phenol, chlorophenols, bisphenol A and alkylphenols are categorized as one of the group compounds belonged to EDCs and have been named as priority pollutants by the United States Environmental Protection Agency (USEPA) (Horikoshi *et al.*, 2002;

Pera-Titus *et al.*, 2004; Ray *et al.*, 2009; Ma *et al.*, 2012a). In addition, the contamination of these phenols in surface waters has also been reported in several countries (Abdullah and Nainggolan, 1991; Schmidt-Bäumler *et al.*, 1999; Gao *et al.*, 2008; Zhong *et al.*, 2010; Santhi *et al.*, 2012). In Malaysia, phenols have been detected at concentrations ranging from 0.8–53.6 µg/L in the Linggi River, Negeri Sembilan. The major sources of detected phenols have been identified as effluents from rubber processing factories, timber sawmills, motor and battery workshops, engineering workshops, pig farming and agricultural activities. The levels of phenols in Linggi River were also found to exceed the recommended Malaysian standard of 2.0 µg/L for raw water (Abdullah and Nainggolan, 1991). Therefore, to overcome the wastewater pollution problems and to comply with the strict environmental regulation, scientist and researchers have focused on the development of new or more effective wastewater treatment technologies so as to convert the organic pollutants into simpler and harmless compounds to eliminate the environmental pollution.

A variety of conventional biological, chemical and physical methods are presently available to treat the harmful compounds in the effluents. However, these conventional wastewater treatments have limitations of their own in order to reach the degree of purity required for final use. Figure 1.1 presents a schematic representation of different treatment technologies. Biological treatment by living organisms is the most widely used for handling various types of aqueous organic pollutants. However, some pollutants such as halogenated organic compounds present in the industrial effluent are found not readily biodegradable and may kill the active microbes (Sanromán *et al.*, 2004). Chlorination is a common chemical oxidation technology in the conventional wastewater treatment process. However, the chlorination based treatment process gave a particular problem where the chlorinated

organic compounds as by-products can be generated after the chlorination treatment (Moonsiri *et al.*, 2004). Conventional physical treatments such as air stripping and activated carbon adsorption have also been employed. Nonetheless, these processes are non-destructive and usually comprised a simple transfer of the pollutants from one phase to another phase (Rezaei and Habibi-Yangjeh, 2013), thus causing secondary pollution. On the other hand, a relatively new class of technologies known as Advanced Oxidation Processes (AOPs) evolved from research works have been considered to overcome many limitations of conventional wastewater treatment.

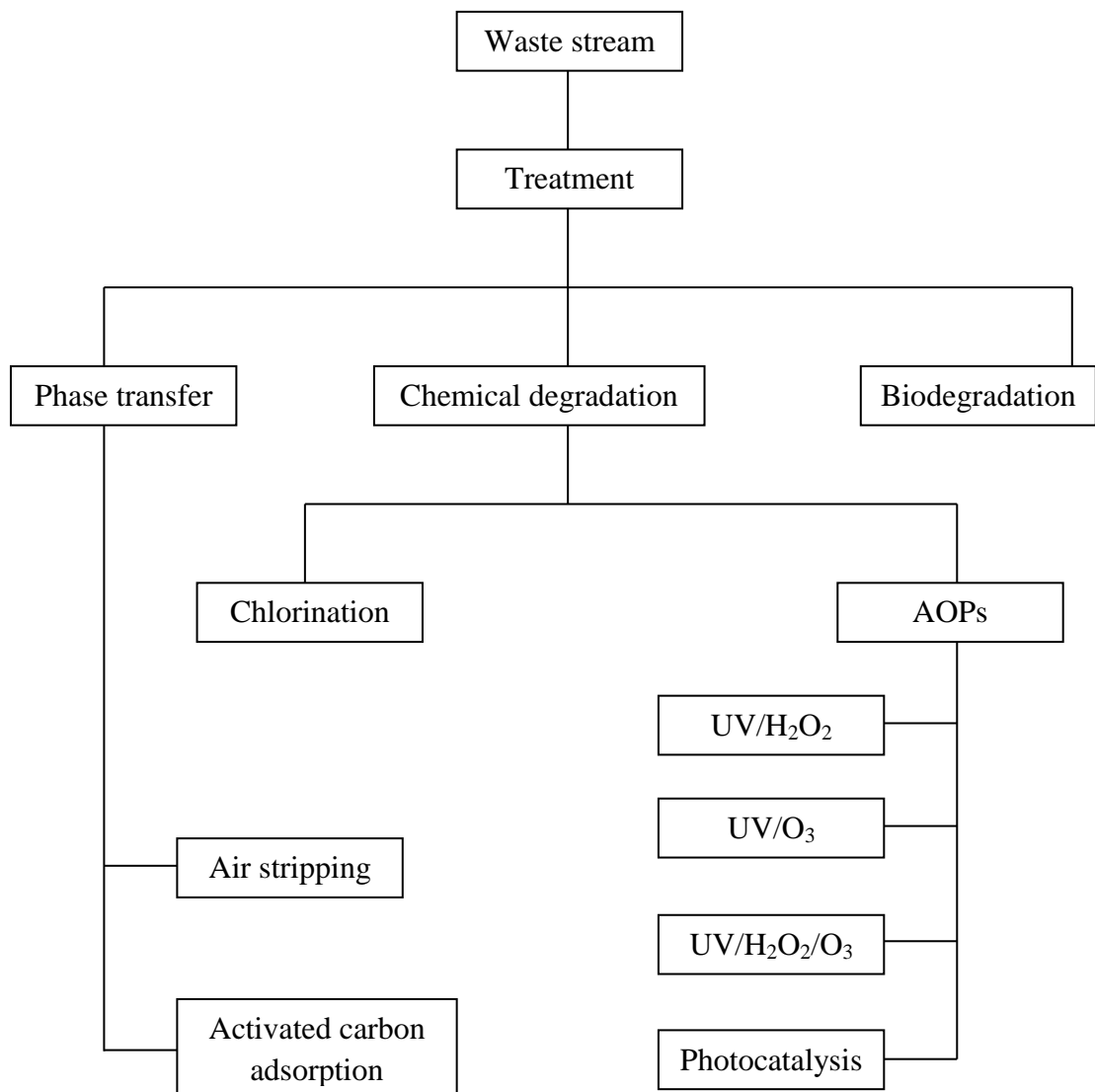


Figure 1.1: Different wastewater treatment technologies currently in use in environmental remediation (Visvanathan *et al.*, 2005; Mohan and Pittman, 2006; An *et al.*, 2010).

1.2 PHOTOCATALYSIS IN WASTEWATER TREATMENT

The advances in chemical wastewater treatment have led to the development of a range of technologies termed as Advanced Oxidation Processes (AOPs). AOPs have been defined broadly as oxidation processes which are primarily based on the in-situ generation of highly reactive transitory oxygen contained radicals such as hydroxyl radicals ($\bullet\text{OH}$) or superoxide anion radicals ($\text{O}_2\bullet^-$) in the mechanisms resulting in the degradation of organic pollutants (An *et al.*, 2010; Khataee and Kasiri, 2010). Some of the processes to obtain these radicals are UV/ H_2O_2 , UV/ O_3 , UV/ $\text{H}_2\text{O}_2/\text{O}_3$ and photocatalysis. Among the AOPs, heterogeneous photocatalysis has recently been accepted as a promising new alternative in the area of wastewater treatment. Photocatalysis differed from the other AOPs because it can use reusable semiconducting catalysts in combination with low energy UV-A light, and it does not require the addition of any other strong oxidants. The advantages of photocatalysis over other conventional methods can be summarized as follows (Yu *et al.*, 2007; Malato *et al.*, 2009):

1. Photocatalytic reactions can occur under ambient temperature and pressure.
2. Degradation of a wide variety of organic pollutants in both aqueous and gaseous systems has been demonstrated.
3. Pollutants are not merely transferred from one phase to another, but they are chemically transformed and completely mineralized to environmentally harmless compounds.
4. Atmospheric oxygen is used as oxidant and no other oxidant is required.

5. The photocatalysts are easily available, inexpensive, non-toxic and can be reused.
6. The photocatalyst activation can happen under low energy UV-A light and even natural sunlight.

Titanium dioxide (TiO₂) is among the semiconductor materials that has been the most investigated as photocatalyst due to its high photocatalytic ability in the wastewater treatment. Nevertheless, the extensive use of TiO₂ is uneconomical for large-scale wastewater treatment (Kansal *et al.*, 2007). Given the drawbacks to the application of TiO₂ in the waste remediation, there is renewed interest to seek for suitable alternatives to TiO₂. Recently, ZnO has been received great attention from many researchers as a suitable alternative to TiO₂. It is because ZnO has high photosensitivity, large band gap, non-toxic nature, and its photocatalytic degradation mechanism is also similar to that of TiO₂ (Sakthivel *et al.*, 2003; Ravichandran *et al.*, 2007; Kansal *et al.*, 2010). In some cases, ZnO has actually proven more effective than TiO₂ (Khodja *et al.*, 2001; Sakthivel *et al.*, 2003; Kansal *et al.*, 2009; Li *et al.*, 2010; Peng *et al.*, 2013). The ZnO-mediated photocatalysis process has been successfully used to degrade many organic pollutants for the past few years (Khodja *et al.*, 2001; Sakthivel *et al.*, 2003; Daneshvar *et al.*, 2007a; Kansal *et al.*, 2009; Elmolla and Chaudhuri, 2010; Li *et al.*, 2010; Liu *et al.*, 2012; Peng *et al.*, 2013). In addition, ZnO is available at low cost, which provided it an important advantage (Bitenc *et al.*, 2013). Nevertheless, the photocatalytic activity of ZnO is limited to UV irradiation as the band gap of ZnO is ~3.3 eV and only 3-5% of the whole solar energy is effectively used, while 43% of the visible light is opened to exploit (Liu *et al.*, 2013). Therefore, many researchers attempted to extend the light absorption of ZnO to higher wavelengths to circumvent this drawback.

1.3 PROBLEM STATEMENT

Phenol and 2,4-dichlorophenol (2,4-DCP) have attracted great concerns nowadays because they can disrupt the normal regulatory function of the endocrine systems. Several adverse effects such as infertility, abnormal sexual development, immune suppression and varieties of cancers have been reported can be induced by these EDCs (Fawell and Hunt, 1988; Zhang *et al.*, 2008; Olujimi *et al.*, 2010; Ma *et al.*, 2012a). Phenols are present in the effluents of various industries such as petrochemical industry (2.8–1220 mg/L), coking operations (28–3900 mg/L), coal processing (9–6800 mg/L) and refineries (6–500 mg/L). Other sources of waste stream containing phenols are pharmaceutical, plastics, wood products, paint and pulp and paper industries (0.1–1600 mg/L) (Busca *et al.*, 2008). The leakage of these EDCs to the environment has also been reported by many researchers (Gao *et al.*, 2008; Zhong *et al.*, 2010). Therefore, there is a need to develop treatment methods that are effective in eliminating these EDCs.

The ZnO-mediated photocatalysis has been found to be one of the most promising methods for degradation of various organic pollutants including phenols (Khodja *et al.*, 2001; Pardeshi and Patil, 2008; Gaya *et al.*, 2009). Since a photocatalysis reaction mainly occurred at the interface between ZnO surfaces and organic pollutants, the morphology of the photocatalysts can play an important role in determining catalytic performance properties. Thus, much effort has been devoted to the synthesis of ZnO with different morphologies and structures, such as nanorods, nanowires, nanosheets, nanocapsules, hierarchical and complex ZnO micro/nanoarchitectures to effectively degrade numerous organic pollutants (Kang *et al.*, 2010; Wu and Huang, 2010; Lu *et al.*, 2011a; Khayyat *et al.*, 2012; Peng *et al.*, 2013). Recently, three-dimensional (3D) hierarchical ZnO architectures which are

assembled from low dimensional nanoscaled building blocks have attracted considerable attentions (Lu *et al.*, 2011a; Lei *et al.*, 2012; Li *et al.*, 2012). Compared to low dimensional ZnO structures, the 3D hierarchical ZnO micro/nanoarchitectures exhibited improved photocatalytic activity due to their higher surface areas and stability against aggregation (Lei *et al.*, 2012; Xu and Mei, 2013). In addition, the larger size of hierarchical ZnO micro/nanoarchitectures can also easy to be separated from the solution after the photocatalytic reactions (Lei *et al.*, 2012; Hong *et al.*, 2013).

Moreover, due to its wide band gap (~3.3 eV), ZnO required UV illumination to activate it, which only represented a small portion 3–5% of sunlight. This indicated that more energy is needed to supply light of appropriate wavelength and this could make the use of photocatalytic technology became expensive. The photocatalytic activity of ZnO is also suffered from fast recombination of photogenerated electron–hole ($e_{cb}^- - h_{vb}^+$) pairs, which affected the photocatalytic efficiency (Sun *et al.*, 2011; Liu *et al.*, 2013). These disadvantages of ZnO forestalled this technique in the practical applications. To address this lapse, modifications of ZnO photocatalysts including doping of metal or non-metal ions, deposition of noble metals as well as use of coupled semiconductors have been reported (Zhang and Zeng, 2010; Khatamian *et al.*, 2012; Liu *et al.*, 2013; Qiu *et al.*, 2013). Recently, some studies have reported doping with rare earth (RE) ions was a useful way for improving the above two performances of ZnO (Karunakaran *et al.*, 2010; Khatamian *et al.*, 2012; Yayapao *et al.*, 2013a). The doping of RE ions on the ZnO produced impurity energy levels in band gap and expanded its light response; furthermore, it produced traps for photogenerated charge carriers, thus inhibiting the recombination

of $e_{cb}^- - h_{vb}^+$ pairs and improving the photocatalytic efficiency (Khatamian *et al.*, 2012; Yayapao *et al.*, 2013a).

On the basis of the above consideration, this study focused on the synthesis of 3D ZnO hierarchical micro/nanospheres by a chemical precipitation method. This study also intended to further improve the photocatalytic efficiency of the synthesized ZnO by adding dopants. Investigated dopants were RE ions and in this study, three different RE ions (RE ion = cerium (Ce), europium (Eu) and neodymium (Nd)) were used. Their photocatalytic activities were investigated on the degradation of phenol and 2,4-DCP under fluorescent light and sunlight irradiation. The photocatalytic activity performed using the fluorescent light available from ordinary compact fluorescent lamp could provide the opportunities for the photocatalysis application in indoor environments. On the other hand, the use of sunlight in the photocatalytic activity could be beneficial to our country as Malaysia is an equatorial climate country where abundant and clean solar energy is available for organic pollutants degradation.

1.4 RESEARCH OBJECTIVES

The aim of this study is to investigate the photocatalytic degradation of phenol and 2,4-dichlorophenol (2,4-DCP) using the rare earth (RE)-doped ZnO hierarchical micro/nanospheres. From the viewpoint of practical applications, utilization of indoor fluorescent light and sunlight is desirable. Hence, the objectives of this research are:

1. To synthesize pure and RE-doped ZnO hierarchical micro/nanospheres (RE/ZnO, RE ion = Ce, Eu and Nd) using a chemical precipitation method.

2. To characterize the chemical, physical and optical properties of the synthesized photocatalysts.
3. To study the photocatalytic performance of the synthesized photocatalysts on the degradation of phenol and 2,4-DCP under fluorescent light and sunlight irradiation.
4. To identify the by-products of the reaction and to propose pathway of phenol and 2,4-DCP degradation.
5. To investigate the kinetics and electrical energy efficiencies in the photocatalytic degradation of phenol and 2,4-DCP.

1.5 SCOPE OF STUDY

This research is focused on the development of RE-doped ZnO hierarchical micro/nanospheres (RE/ZnO, RE ion = Ce, Eu and Nd) using a chemical precipitation method for the photocatalytic degradation of phenol and 2,4-DCP under fluorescent light and sunlight irradiation. The development of the RE/ZnO included studying the effects of RE doping content and calcination temperature. The developed photocatalysts are characterized by X-ray diffraction (XRD), scanning electron microscopy (SEM), energy dispersive X-ray (EDX) spectroscopy, transmission electron microscopy (TEM), high-resolution transmission electron microscopy (HRTEM), UV–visible diffuse reflectance spectroscopy (UV-vis DRS) and N₂ adsorption-desorption. Moreover, the morphology evolution and the mechanism on the formation of such ZnO hierarchical structures are also studied. Meanwhile, the comparison photocatalytic studies with commercial TiO₂ and ZnO nanorods (ZNRs) prepared by the solvothermal method are also conducted. The proposed photocatalytic mechanism of RE/ZnO is studied by means of adding radical

scavengers, photoluminescence (PL) spectra and terephthalic acid-photoluminescence (TA-PL) analysis.

The operating parameters such as initial substrate concentration and solution pH on the photocatalytic degradation of phenol and 2,4-DCP are studied. The evolution of reaction intermediates during the photocatalytic degradation of phenol and 2,4-DCP is monitored using a high performance liquid chromatography (HPLC) while the extent of mineralization is monitored using total organic carbon (TOC) analyzer and ion chromatography. The kinetic studies are further carried out to obtain the reaction order, rate constant and reaction rate on the photodegradation of phenol and 2,4-DCP. Finally, the evaluation of electrical energy per order (E_{EO}) for photocatalytic degradation of phenol and 2,4-DCP is performed using the synthesized photocatalysts.

1.6 ORGANIZATION OF THESIS

There are five chapters in this thesis. Chapter 1 (Introduction) provides a brief description of wastewater treatment and photocatalysis in wastewater treatment. This chapter also includes the problem statement that describes the problem faced and the needs of the current research. The objectives and the scopes of this study are then explained in this chapter. This is followed by the organization of the thesis.

Chapter 2 (Literature Review) provides the past research works in the photocatalysis field. Brief explanation about ZnO, their properties and basic principles of ZnO photocatalysis are in the first part. Subsequently, information regarding with the ways modifying the ZnO photocatalysts and ZnO photocatalysts preparation are discussed in the second part. Next, the effects of operating parameters

that affect the photocatalytic activity are included. Finally, the characteristics of phenol and 2,4-DCP as well as the details of their degradation are described.

Chapter 3 (Materials and Methods) covers the experimental part. Details of the materials and chemical reagents and the research methodology used in the present study are described. Detailed of the experimental setup including a step-wise description of the photocatalyst synthesis, photocatalyst characterizations, photocatalytic performance evaluation and sample analyses are also outlined in this chapter.

Chapter 4 (Results and Discussion) presents the experimental findings together with discussion. It is divided into eight parts, which are (a) characterization of the as-synthesized rare earth-doped ZnO hierarchical micro/nanospheres (RE/ZnO), (b) investigation of the formation of such ZnO hierarchical structures, (c) effects of RE doping content and calcination temperature on the photocatalytic activity of RE/ZnO, (d) photocatalytic mechanism study of RE/ZnO, (e) effects of operating parameters on the photocatalytic degradation of phenol and 2,4-DCP, (f) reaction mechanisms for phenol and 2,4-DCP degradation, (g) kinetic studies and (h) electrical energy evaluation.

Chapter 5 (Conclusions and Recommendations) summarizes the results reported in chapter 4 and recommends the possible ways to improve the present studies for future research in this field.

CHAPTER TWO

LITERATURE REVIEW

2.1 ENDOCRINE DISRUPTING CHEMICALS

Disruption of the endocrine system in wildlife and human by anthropogenic chemicals has become an issue of worldwide concern due to the recognition of that the environment is contaminated with various endocrine disrupting chemicals (EDCs) that exert hormonal imbalance activity (Gültekin and Ince, 2007). In 1996, the European Commission has defined the EDC as an exogenous substance or a mixture that alters the function of the endocrine system and consequently causes adverse health effects in an organism or its progeny or (sub) populations (Krieger, 2001). To date, there is a wide range of compounds that have been recognized as EDCs through laboratory studies. They included a plethora of industrial chemicals such as phenols, dioxins, pesticides, parabens, phthalates, polycyclic aromatic hydrocarbons (PAHs), brominated flame retardants and some heavy metals (Belgiorno *et al.*, 2007; Gültekin and Ince, 2007; Caliman and Gavrilesco, 2009; Olujimi *et al.*, 2010).

The EDCs can interact with the hormone receptors and altered the natural response patterns of the endocrine system (Figure 2.1). The EDCs may bind to the receptor and activated responses, therefore acting as hormone mimic. This is termed as an agonistic effect. In other way, the EDCs may bind to receptor, but no response is generated and also blocked the natural hormone from interacting. This is defined as an antagonistic effect (Nicolopoulou-Stamati and Pitsos, 2001; Birkett and Lester, 2003). According to Gültekin and Ince (2007), the three major endocrine disruption endpoints were estrogenic (compounds that mimicked or blocked natural estrogens), androgenic (compounds that mimicked or blocked natural testosterone) and thyroidal

(compounds with direct and/or indirect impacted on the thyroid). Some of the adverse health effects that can be occurred in the endocrine system by the EDCs were hormone-dependent cancers, reproductive system disorders and reduction in reproductive fitness. In fact, enormous examples of reproductive and developmental abnormalities have been reported over the years in a broad spectrum of wildlife including fish, amphibians, birds and mammals (Fawell and Hunt, 1988; Aoyama *et al.*, 2005; Ma *et al.*, 2012a), many of which were associated with EDCs exposure.

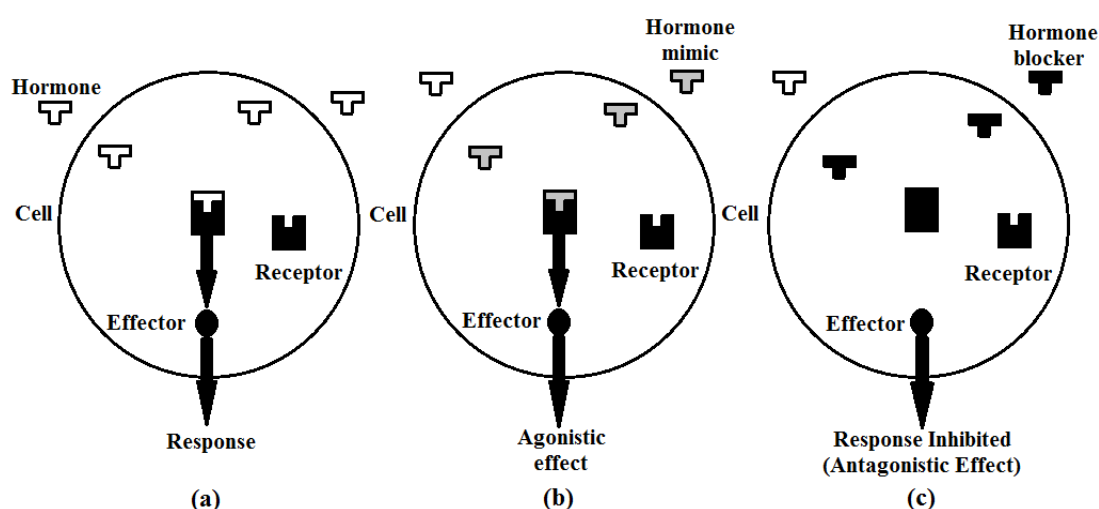


Figure 2.1: Endocrine disruption processes: (a) Natural response, (b) agonistic effect and (c) antagonistic effect (Birkett and Lester, 2003).

Widespread occurrences of EDCs in the environment have been reported in many countries (Schmidt-Bäumler *et al.*, 1999; Gao *et al.*, 2008; Zhong *et al.*, 2010). Sources by which EDCs contaminated the surface water are via sewage effluents from domestic and industrial facilities and industrial effluent discharges. The quantity of chemicals within the aquatic environment together with the inherent susceptibility of aquatic life to the effects of EDCs, leads to significant impacts on the biota of aquatic ecosystems. In certain water bodies, the EDCs concentrations have been reported in the range from $\mu\text{g/L}$ to mg/L (Schmidt-Bäumler *et al.*, 1999; Gao *et al.*, 2008). Despite their low concentrations present in the aquatic environment,

the EDCs have been listed as hazardous pollutants by USEPA due to the fact that even a trace amount of them is highly carcinogenic to human and animals.

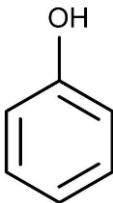
Various chemical, physical and biological treatment processes are currently used for the removal of EDCs. Results showed that the activated sludge wastewater treatment has variable performance in removing EDCs. Baronti *et al.* (2000) reported that the removal efficiencies for estrone (E1) and 17 β -estradiol (E2) were 87% and 61%, respectively. In a study of Svenson *et al.* (2003), the average removal efficiency of estrogenicity in municipal sewage treatment plants was 81% by activated sludge treatment and only 28% by solid supported bacterial treatment. It is therefore essential to install additional treatment processes after secondary treatment step to ensure a more complete removal of EDCs. On the other hand, activated carbon adsorption is a versatile technology for removing EDCs compounds from wastewater. It has been shown to be effective in adsorbing EDC pollutants such as bisphenol A and nonylphenol (Choi *et al.*, 2005). However, activated carbon only transported the EDCs from one medium (water) to another (activated carbon). Consequently, alternative treatment technology has to be sought, among which heterogeneous photocatalysis has recently been accepted as a promising technique for removing EDCs from effluents. Hence, this work is to study on the degradation of two common and widely used phenolic EDCs, namely phenol and 2,4-dichlorophenol (2,4-DCP) by heterogeneous photocatalysis.

2.1.1 Phenol

Phenol is an aromatic component which contained one hydroxyl group that is attached to an aromatic ring as illustrated in Table 2.1. Currently, phenol is produced at a rate of about 6 million ton per year worldwide and the cumene-to-phenol process

is the predominant synthetic route for the production of phenol. Cumene for this process is produced from the alkylation of benzene with propene. Then, cumene is oxidized with oxygen to form cumene hydroperoxide. The peroxide is subsequently decomposed to phenol accompanied by acetone as a co-product (Solomons and Fryhle, 2004; Weber and Weber, 2010). Phenol has a melting point of 40.9°C. In the molten state, pure phenol appeared as a colourless and clear liquid. On exposure to air, phenol rapidly became pink in colour due to certain trace impurities such as iron that present during the production process. Phenol is also soluble in water and organic solvents such as aromatic hydrocarbons, alcohols and ethers (Busca *et al.*, 2008). The physical and chemical properties of phenol are shown in Table 2.1.

Table 2.1: Chemical and physical properties of phenol (Busca *et al.*, 2008).

Chemical structure	
Molar mass	94.11 g/mol
Density	1.07 g/cm ³
Melting point	40.9°C
Boiling point	181.7°C
Water solubility (room temperature)	9.3 g/100 mL
pKa	9.9

Phenol has been widely used in the production of phenolic resins like phenol-formaldehyde resins (Bakelite) which are low cost thermosetting resins applied as plywood adhesive, construction automotive and appliance industries. By reaction with acetone, phenol can convert to bisphenol A, an important substrate in the manufacture of polycarbonate resins. Phenol is also used in the synthesis of caprolactum as a precursor for nylon 6 and other man-made fibers. Phenol is also a building block for the synthesis of pharmaceuticals such as aspirin. In addition,

phenol can also be converted into alkylphenols and chlorophenols in the production of wood preservatives, dyestuffs, agricultural chemicals, surfactants and plastic plasticizers (Myers, 2007; Busca *et al.*, 2008). Due to the extensive use and poor biodegradability of phenol, it has resulted in its ubiquitous presence in the environment. Widespread occurrences of phenol in surface waters have been reported in several countries at concentrations ranging from 0.09–7.80 µg/L (Schmidt-Bäumler *et al.*, 1999; Zhong *et al.*, 2010).

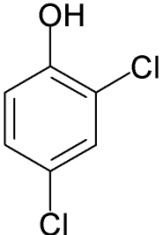
Phenol is an endocrine disrupting chemical with toxicity, carcinogenic and mutagenic properties. Indeed, a dose-related increase in chromosomal aberrations has been reported in spermatogonia and primary spermatocytes of mice treated with solution of phenol (0 to 8.0 mg/L) in water in multigeneration studies. The phenol-induced chromosomal aberrations were also reported to be increased in intensity with succeeding generations (Fawell and Hunt, 1988; Ray *et al.*, 2009). Phenol was also found to be mutagenic to *Salmonella typhimurium* and *Escherichia coli* bacterium (Fawell and Hunt, 1988). Increase incidence of leukaemia, depression of body weight gain and decrease of water consumption were also reported on rats after given drinking water containing 2.5 to 5.0 g/L phenol for 103 weeks (Fawell and Hunt, 1988). On the other hand, phenol has relevant health effects for humans. Phenol is rapidly adsorbed through the human skin and can burn the skin and eye upon contact. Central nervous system, liver, kidneys, pancreas can also be affected by ingesting the water contaminated with phenol. In addition, the ingestion of 1 gram of phenol can have fatal consequences in humans (Busca *et al.*, 2008; Hameed and Rahman, 2008). Due to its hazardous nature, phenol has been listed as priority pollutant by USEPA. The strict standards were also passed because of its effect to human health. The World Health Organization (WHO) has recommended that the phenol concentration

in water resources entering conventional water treatment must be $<2 \mu\text{g/L}$. Moreover, the concentration of phenol in drinking water must be $<0.1 \mu\text{g/L}$ (Schmidt-Bäumler *et al.*, 1999; Nickheslat *et al.*, 2013).

2.1.2 2,4-dichlorophenol (2,4-DCP)

Extensive use of chlorophenols as pesticides, disinfectants, wood treatment agents and as a byproduct of bleaching in paper mills have led to chlorophenols being distributed in the environment (Zhang *et al.*, 2008; Pohanish, 2012). Because the chlorophenols can cause serious problems due to their toxicity, carcinogenicity and adverse effects on human as well as wildlife, the USEPA has classified the pentachlorophenol (PCP), 2,4,6-trichlorophenol (2,4,6-TCP) and 2,4-DCP as priority pollutants (Liu *et al.*, 2012b; Ba-Abbad *et al.*, 2013). Of these chemicals, 2,4-DCP is the most abundant in aquatic environments (Zhang *et al.*, 2008). 2,4-DCP is primarily formed as a biotransformation product of the pesticide 2,4-dichlorophenoxyacetic acid and is also derived as a degradation product of more chlorinated chlorophenols (Ma *et al.*, 2012a). The annual worldwide production of 2,4-DCP was estimated at 88 million pounds and its contamination in surface waters has been observed in many studies in different countries (House *et al.*, 1997; Chiron *et al.*, 2007; Gao *et al.*, 2008). In China, 2,4-DCP have been detected in seven major watersheds and maximum concentrations as great as 19960 ng/L have been reported in Yellow River (Gao *et al.*, 2008). The physical and chemical properties of 2,4-DCP are shown in Table 2.2.

Table 2.2: Chemical and physical properties of 2,4-DCP (Pohanish, 2012).

Chemical structure	
	
Molar mass	163.00 g/mol
Density	1.20 g/cm ³
Melting point	45°C
Boiling point	210°C
Water solubility	Slightly soluble in water
pKa	7.9

The endocrine disrupting effect of 2,4-DCP has been reported on the reproductive toxicity in rats (Aoyama *et al.*, 2005). In their study, the rats were given diet containing 2,4-DCP at dose levels ranging from 0–8000 ppm to investigate the potential effects of the 2,4-DCP on parental animals and their offspring over two successive generations. The results showed that the body weight and the food consumption of both males and females were significantly affected in 2000–8000 ppm 2,4-DCP. The reproductive effects including increased uterine weights as well as reduced number of implantation sites and live births also occurred in the exposure of 2000–8000 ppm 2,4-DCP. A study by Ma *et al.* (2012a) also found that the exposure of zebrafish to 2,4-DCP resulted in lesser rates of hatching of eggs. Their results also demonstrated that 2,4-DCP modulated transcription of steroidogenic genes in the zebrafish and disrupted steroidogenesis, which in turn caused adverse effects on reproduction in fish. Similar results were also reported by Zhang *et al.* (2008) on the effect of 2,4-DCP to minnow. They stated that 2,4-DCP can be a potential endocrine disruptor and caused adverse effects in female sex organs through interruption of the estrogen receptor. On the contrary, short term exposure of 2,4-

DCP also can cause skin irradiation, while long term exposure may cause liver and kidney damage and may affect the nervous system causing headache, dizziness, vomiting, weakness and possible coma (Pohanish, 2012).

2.2 HETEROGENEOUS PHOTOCATALYSIS

Heterogeneous photocatalysis has been intensively studied within the last four decades and shown to be an effective means of removing a wide range of organic pollutants both in air and water media. It can be defined as the acceleration of a chemical reaction in the presence of light and catalyst. As semiconductor shows a band gap, which extends from the filled valence band (VB) to vacant conduction band (CB), it can be used as a photocatalyst. Activation of a semiconductor photocatalyst can be obtained via the absorption of photon with energy equal to or greater than its band gap which resulted in the promotion of an electron (e_{cb}^-) from the VB into the CB, leaving behind a hole (h_{vb}^+) in the VB (Lasa *et al.*, 2006; Gaya and Abdullah, 2008; Bingham and Daoud, 2011). Figure 2.2 shows the photoexcitation of e_{cb}^- from the filled VB to the vacant CB.

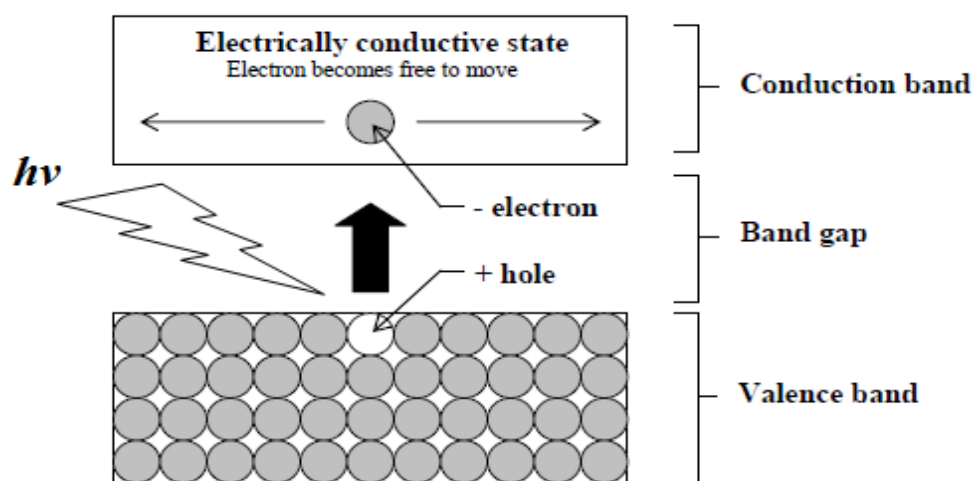


Figure 2.2: Photoactivation of the electron within the bandgap (Gaya and Abdullah, 2008).

Once excitation of the semiconductor happened across the band gap, the photogenerated e_{cb}^- - h_{vb}^+ pair can undergo charge transfer to adsorbed species on the semiconductor surface. Figure 2.3 displays the schematic photoexcitation of the semiconductor photocatalyst and the following redox reactions. Migration of e_{cb}^- and h_{vb}^+ to the semiconductor surface is followed by transfer of photogenerated e_{cb}^- to adsorbed species. The e_{cb}^- transfer process is more efficient if the species are pre-adsorbed on the semiconductor surface. While at the surface of semiconductor, e_{cb}^- is donated to reduce an electron acceptor (pathway C). On the other hand, h_{vb}^+ can migrate to the surface, where it can combine with electron from donor species to oxidize the donor species (pathway D) (Tariq *et al.*, 2005; Koči *et al.*, 2008). The rate of the charge transfer processes for e_{cb}^- and h_{vb}^+ depended upon the respective positions of the band edges for the CB and VB and the redox potential levels of the adsorbate species. As a result of the redox reactions, reactive and strongly oxidizing radicals can form and responsible for degradation of numerous organic pollutants. In competition with charge transfer to adsorbed species is e_{cb}^- and h_{vb}^+ recombination. Recombination can occur in the volume and at the surface of semiconductor photocatalyst with a characteristic time of 10 to 100 ns (pathways A and B) (Herrmann, 2005).

In a heterogeneous photocatalytic process, the reaction itself happened in the adsorbed phase and Herrmann (2005) suggested that the overall classical heterogeneous photocatalytic process can be divided into five independent steps:

1. Diffusion of reactants to the surface of catalyst.
2. Adsorption of one of the reactants.
3. Reaction of the reactants in the adsorbed phase.
4. Desorption of products off the surface.

5. Removal of the products from the interfacial region.

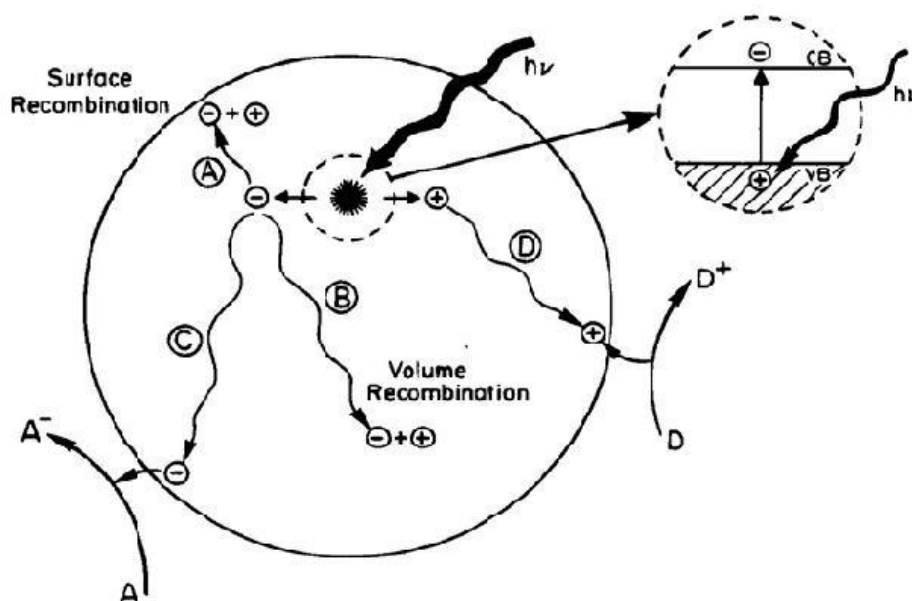


Figure 2.3: Schematic photoexcitation of the semiconductor photocatalyst and the following redox reactions (Koči *et al.*, 2008).

2.3 ZnO AS A PHOTOCATALYST

The absorption of light with appropriate energy by a semiconductor promoted the formation of $e_{cb}^- - h_{vb}^+$ pair. According to the thermodynamic requirement, in order to photooxidize a chemical species, the potential of the VB of the semiconductor should be sufficiently positive than the oxidation potential of the chemical species and to photoreduce a chemical species, the potential of the CB of the semiconductor should be sufficiently negative than the reduction potential of the chemical species. For a semiconductor, in order to be an efficient photocatalyst for photocatalytic reactions, the VB and CB of the photocatalyst should be positioned in such a way that the oxidation potential of the $\bullet\text{OH}$ radical ($E^\circ(\text{H}_2\text{O}/\bullet\text{OH}) = 2.72$ V vs. NHE) and the reduction potential of $\text{O}_2\bullet^-$ radical ($E^\circ(\text{O}_2/\text{O}_2\bullet^-) = -0.33$ V vs. NHE) lay well

within the band gap (Rehman *et al.*, 2009; Vinu and Madras, 2010). Figure 2.4 shows the band positions of various semiconductor photocatalysts and their band gap energy. It is clear that ZnO exhibited favourable band gap position and thus is one of the suitable materials to initiate a photocatalytic process.

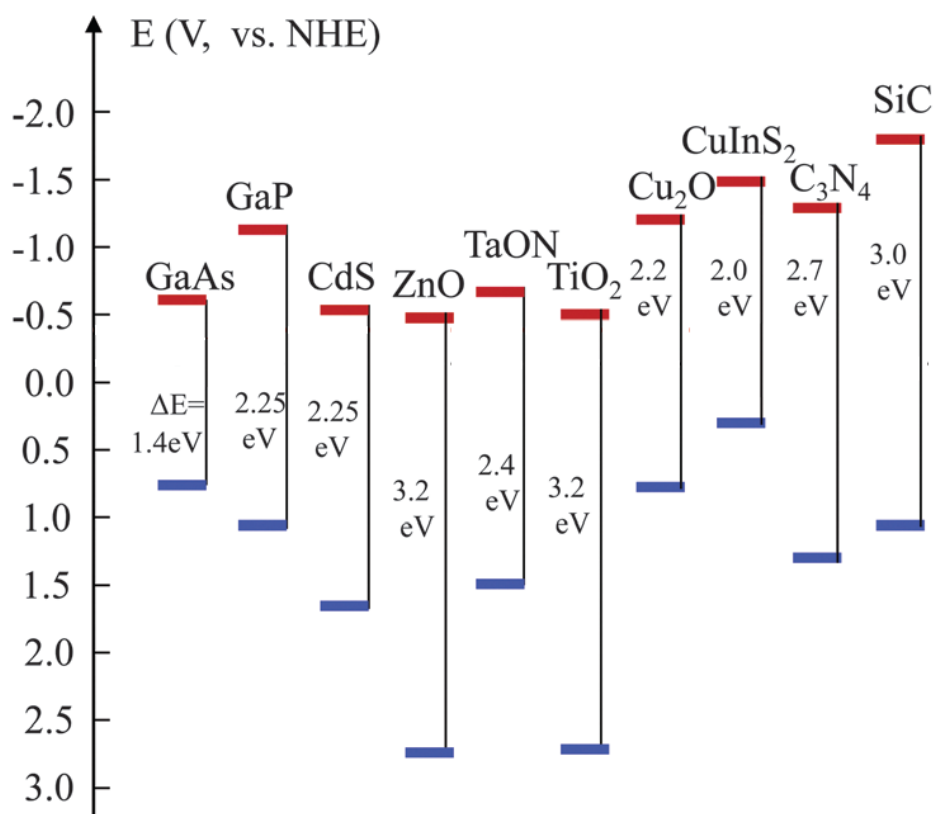


Figure 2.4: The CB and VB positions of some common semiconductor photocatalysts and their band gap energy (Liu *et al.*, 2014).

2.3.1 Basic knowledge of ZnO

There has been a great deal of interest in ZnO lately, as seen from a surge of a relevant number of publications (Krishnamoorthy and Llidis, 2006; Chakraborty *et al.*, 2009; Janotti and Van de Walle, 2009; Umar, 2009; Mahmoud and Al-Ghamdi, 2010; Godlewski *et al.*, 2011; Arya *et al.*, 2012; Rajabi *et al.*, 2013). The interest in

ZnO is fueled and fanned by its various exotic properties such as wide band gap (~3.3 eV), large exciton binding energy, good transparency, biocompatibility and so on (Janotti and Van de Walle, 2009; Umar, 2009). For this reason, ZnO has a significant potential application in the opto-electronic devices (Chakraborty *et al.*, 2009; Godlewski *et al.*, 2011; Rajabi *et al.*, 2013). ZnO has shown several other optical and electro-optical applications in optical switches, optical waveguide and acousto-optic and surface-acoustic applications (Krishnamoorthy and Llidis, 2006; Mahmoud and Al-Ghamdi, 2010; Jiang *et al.*, 2012). ZnO is also an important material for applications in chemical and biosensors, solar cells and photocatalysis (Xu *et al.*, 2011a; Arya *et al.*, 2012; Gu érin *et al.*, 2012).

Physically, ZnO has the appearance of a white powder and is referred to as zinc white or zincite. It usually occurs in crystalline form that is almost insoluble in water and alcohol. ZnO has a molecular mass of 81.40 g/mol and both of its melting point and boiling point are 1975°C. The mineral form of ZnO is usually orange or red in colour due to the presence of impurities such as manganese and other elements. ZnO exhibited amphoteric properties and it is also a typical kind of II-VI compound semiconductor as zinc belonged to the second group and oxygen belonged to the sixth group of the periodical table (Ellmer and Klein, 2008).

Generally, ZnO crystallized in a hexagonal wurtzite structure (Figure 2.5) with lattice parameters $a = 3.25 \text{ \AA}$ and $c = 5.20 \text{ \AA}$ at ambient temperature and pressure. The structure of ZnO can be simply expressed as a number of alternating planes composed of tetrahedrally coordinated O^{2-} and Zn^{2+} ions stacked alternatively along the c -axis (Baruah and Dutta, 2009). Although the wurtzite structure of ZnO is a thermodynamically stable phase, two other structures of ZnO also existed, which are known as the cubic zinc blende and the cubic rocksalt, as schematically shown in

Figure 2.5 (Özgür *et al.*, 2005). In the cubic rocksalt, each anion is surrounded by six cations at the corners of an octahedron; while in the cubic zinc blende and hexagonal wurtzite structure, each anion is surrounded by four cations at the corners of a tetrahedron. Both of these cubic phases are metastable and only occurred under certain conditions such as the zinc blende structure is obtained by growing ZnO on a cubic substrate while the rocksalt structure is achieved from wurtzite structure at relatively high pressures (~ 9 GPa at 300 K) (Özgür *et al.*, 2005; Özgür and Morkoç 2009). For this reason, ZnO has a strong natural tendency to crystallize in the wurtzite structure and therefore nearly all photocatalytic studies are focused on this structure.

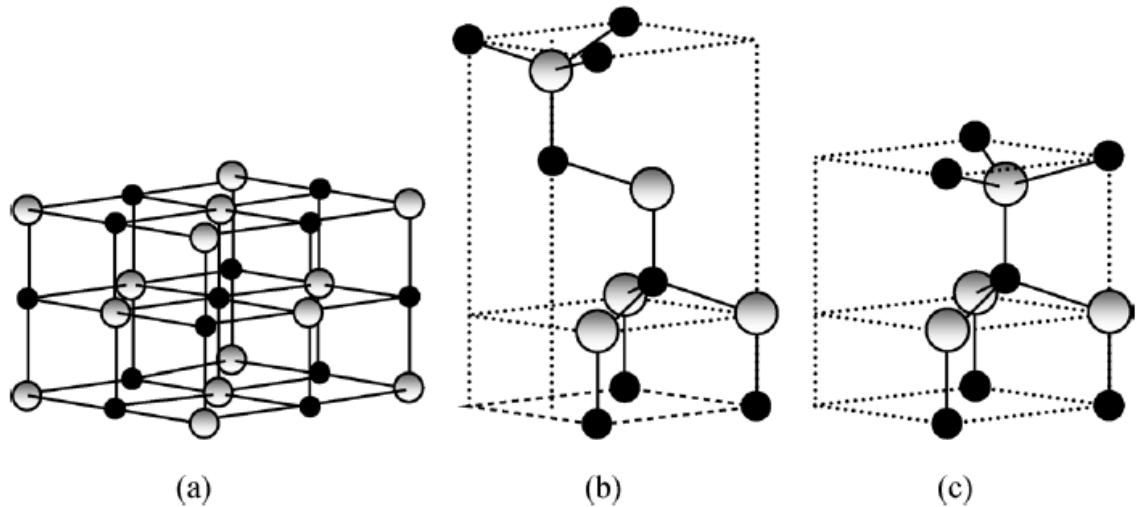


Figure 2.5: Ball and stick representation of ZnO crystal structures: (a) cubic rocksalt; (b) cubic zinc blende; (c) hexagonal wurtzite. The shaded white and black spheres denote Zn and O atoms, respectively (Özgür *et al.*, 2005).